Ozone and NO_2 variations measured during the 1 August 2008 solar eclipse above Eureka, Canada with a UV-visible spectrometer

Cristen Adams,[1] Chris A. McLinden,[2] Kimberly Strong,[1] and Vasil Umlenski[3]

Received 27 April 2010; revised 10 June 2010; accepted 18 June 2010; published 13 October 2010.

[1] On 1 August 2008, a solar eclipse of 98% totality passed over the Polar Environment Atmospheric Research Laboratory at Eureka, Canada (80.05°N, 86.42°W), which is run by the Canadian Network for the Detection of Atmospheric Change. During the eclipse, a zenith-sky UV-visible spectrometer measured slant column densities (SCDs) and vertical column densities (VCDs) of ozone up to 82% occultation and NO_2 up to 96% occultation, beyond which low light intensities and changes in the solar spectrum due to limb darkening compromised data quality. Ozone VCDs during the eclipse remained within natural variability, and this study is inconclusive regarding ozone oscillations due to limited temporal resolution and measurement errors toward eclipse maximum. Measured NO_2 SCDs increased and decreased symmetrically around the eclipse maximum. NO_2 SCDs were also calculated using a photochemical box model and a one-dimensional radiative transfer model. The modeled ratio of eclipse day SCDs to the previous day's SCDs was compared to the measurements. They agreed within error bars leading up to maximum occultation, but the model ratio was systematically larger than the measured ratio for the second half of the eclipse, perhaps due to changing cloud conditions throughout the eclipse. The measured NO_2 SCD ratio of $1.84^{+0.12}_{-0.43}$ at 96% totality is larger than observed in past studies and agrees with modeled ratio of 1.91. Therefore our current understanding of stratospheric photochemistry is sufficient to predict the evolution of NO_x chemistry through a solar eclipse.

Citation: Adams, C., C. A. McLinden, K. Strong, and V. Umlenski (2010), Ozone and NO_2 variations measured during the 1 August 2008 solar eclipse above Eureka, Canada with a UV-visible spectrometer, *J. Geophys. Res.*, *115*, D19310, doi:10.1029/2010JD014424.

1. Introduction

[2] Solar eclipses provide a rare opportunity to study atmospheric photochemistry: during an eclipse, the Moon extinguishes sunlight to all layers of the atmosphere in a short time compared to sunset, during which the sunlight is gradually extinguished layer by layer. However, the brightness of the Sun and the solar spectrum as seen from Earth also change rapidly during solar eclipses. Therefore, accurate remote sensing of the atmosphere during a solar eclipse remains a challenge.

[3] Below 30 km, where the bulk of the ozone column resides, ozone has a lifetime of at least a month. Therefore, a 2 h solar eclipse should not lead to significant photochemical changes in the total ozone column. Ozone measurements during eclipses have yielded a variety of results. Brewer and Dobson spectrophotometers have measured both significant increases and decreases in ozone during solar eclipses [e.g., *Bojkov*, 1968; *Chakrabarty et al.*, 2001]. Many of these studies account for the effect of the changing solar spectrum (limb darkening), which is only on the order of 0.01% [*Kazadzis et al.*, 2007], but they do not account for the effects of diffuse radiation during eclipses, which can cause artificial decreases in Brewer and Dobson vertical column densities (VCDs) of up to 30 Dobson units (DU) [*Zerefos et al.*, 2000]. While the Brewer and Dobson spectrophotometer measurements are compromised during eclipses, other instruments have also yielded a variety of results during eclipses, including a 30% decrease in ozone measured by a radiometer [*Dani and Devara*, 2002] and no changes in concentration measured in situ at 19.8 km [*Starr et al.*, 1980]. With a visible spectrometer, *Gil et al.* [2000] found a decrease of approximately 5% in ozone VCD, which was not significant due to measurement uncertainties.

[4] While photochemical changes in ozone are not predicted, reduced sunlight during eclipses cools the atmosphere, which could lead gravity waves to form a bow wave with periods ranging from 20 min to 4 h, depending on the distance from the eclipse maximum [*Chimonas and Hines*,

[1]Department of Physics, University of Toronto, Toronto, Ontario, Canada.
[2]Environment Canada, Toronto, Ontario, Canada.
[3]Bulgarian Academy of Sciences, Institute of Astronomy, Sofia, Bulgaria.

0148-0227/10/2010JD014424

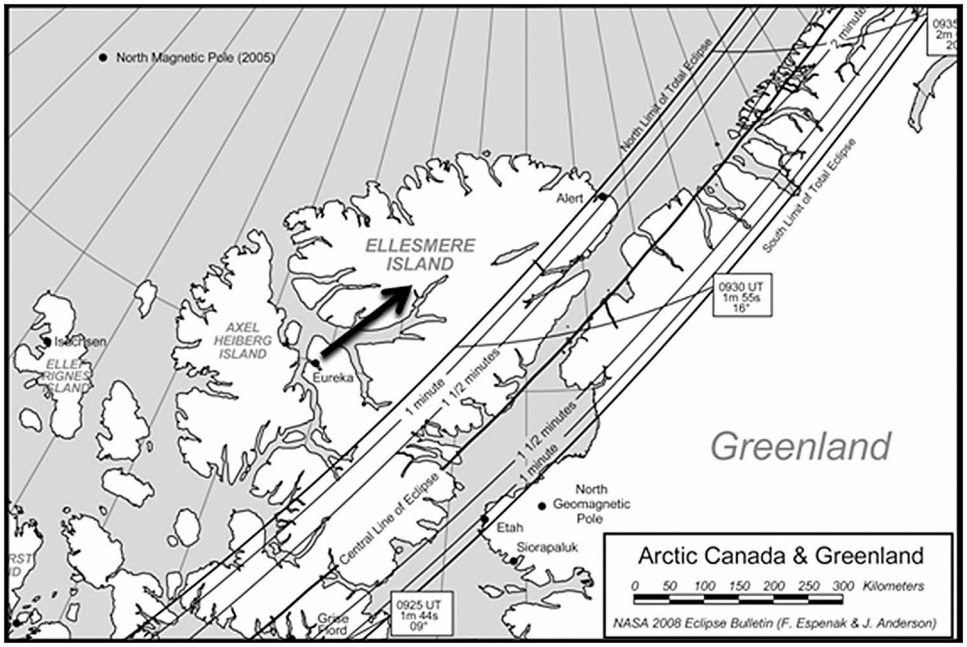

Figure 1. Path of eclipse totality in the Canadian Arctic, courtesy of F. Espenak and J. Anderson at NASA [*Espenak and Anderson*, 2007]. The black arrow marks the line of sight of the PEARL-GBS at the 98% occultation eclipse maximum with solar zenith angle 78°.

1971]. *Fritts and Luo* [1993] modeled eclipse-induced gravity waves and found that variability in the ozone total column would be difficult to detect above background gravity waves but recently *Eckermann et al.* [2007] found that this effect may be larger than previously thought. Several studies have found evidence of waves in ozone measurements, but with varying amplitudes and periods. *Mims and Mims* [1993] smoothed total ozone portable spectrometer measurements by 30% using a fast Fourier transform routine and found an oscillation of 0.1% of the total ozone column with a period of about 7 min, shortly after the eclipse maximum. With a Dobson spectrophotometer, *Chakrabarty et al.* [1997] measured ozone oscillations with an amplitude of about 5% of the total ozone column and a 15 min period but did not correct for limb darkening or increased diffuse radiation. *Dani and Devara* [2002], using a radiometer, measured ozone total column oscillations with amplitudes of ~10% with periods of ~30 min. During a 1999 solar eclipse, *Zerefos et al.* [2000] found evidence of ozone oscillations with periods of about 20 min in erythemal UV-B solar irradiance. In a later study on a 2006 eclipse, *Zerefos et al.* [2007] corrected Brewer data for diffuse radiation and, using spectral Fourier analysis, found total ozone column oscillations with amplitudes of 2.5%–3% and periods of 30–40 min in two Brewer data sets.

[5] Unlike ozone, NO_2 is photochemically active on a time scale of minutes, due to the rapid cycling between NO and NO_2. Theoretically, NO_2 should increase (and NO should decrease) as the Sun is blocked by the Moon until the eclipse maximum, after which both NO_2 and NO should recover to approximately their preeclipse values [*Herman*, 1979; *Wuebbles and Chang*, 1979]. *Pommereau et al.* [1976] first measured an increase in NO_2 during an eclipse using a spectrophotometric technique. *Starr et al.* [1980] measured a decrease of in situ NO at 19.8 km, which agreed well with modeled NO to NO_2 conversion. During an 82% totality eclipse, *Elansky and Arabov* [1983] measured an NO_2 VCD increase of 60% ± 20%, with a direct Sun UV band instrument. During another eclipse of 87% totality, *Elansky and Elokhov* [1993] measured a 55% ± 6% increase in NO_2 VCD using zenith-sky visible spectroscopy. *Chakrabarty et al.* [2001] found that NO_2 slant column densities (SCDs) measured by a visible spectrometer approximately doubled and identified a wavelike structure in the NO_2 measurements. They suggested that the latter effect was related to eclipse-induced gravity waves. *Gil et al.* [2000] used a zenith-sky visible spectrometer and corrected for the changing visible solar spectrum during the eclipse to find a 55% ± 9% NO_2 SCD increase.

2. Measurements and Retrievals

2.1. UV-Visible Measurements

[6] On 1 August 2008, a solar eclipse passed from the Canadian Arctic, over Greenland, and into Asia [*Espenak and Anderson*, 2007]. The path of the eclipse is shown in Figure 1. Above Eureka, Nunavut, the eclipse began at 08:36 UT (03:36 local time), reached a maximum of 98% at 09:30 UT (04:30 local time), and finished at 10:26 UT (05:26 local time). On the morning before the eclipse, 31 July 2008, Environment Canada's Eureka Weather Station recorded mostly cloudy skies, clearing in the afternoon. On the day of the eclipse, the weather was mostly cloudy and rain started to fall around 12 UT (07 local time).

[7] The PEARL-GBS (Polar Environment Atmospheric Research Laboratory Ground-Based Spectrometer) [e.g., *Fraser et al.*, 2008, 2009] is located at PEARL in Eureka, Canada (80.05°N, 86.42°W). It has been operating since

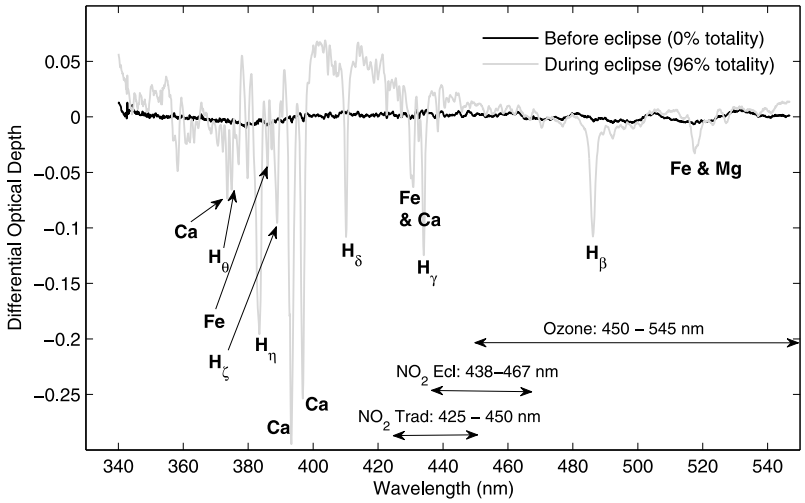

Figure 2. Measured differential optical depths, with no fitting of absorption cross sections, before the eclipse (black) and at 96% totality (gray). The DOAS fitting windows for ozone and NO_2 are indicated (black arrows).

August 2006 as a part of the Canadian Network for the Detection of Atmospheric Change (CANDAC) suite of instruments and makes year-round (light permitting) measurements of ozone and NO_2 differential slant column densities (DSCDs) and VCDs with UV-visible sunlight. The eclipse measurements were taken in the zenith-sky viewing geometry, with a 2° field of view. A 600 g/mm grating yielding a 0.5–2 nm resolution was used. Spectra were recorded with a back-illuminated 2048 × 512 pixel charged-coupled device detector that was thermoelectrically cooled to 202–205 K. To better capture the behavior of ozone and NO_2 during the solar eclipse, the PEARL-GBS measurement frequency was increased from approximately one measurement every 17 min to one measurement every 3 min on the day of the eclipse.

[8] For zenith-sky measurements, the longitude and latitude at which incoming photons are absorbed by trace gases are different from the location of the instrument. Four locations along the line of sight of the instrument were calculated using the method in the work of *Solomon et al.* [1987] and the resulting line of sight of the instrument is marked by the black arrow on Figure 1. The totality of the eclipse versus time for each of these locations was calculated using the formulae in the constant part of the Astronomical calendar [*Abalakin*, 1981]. The angular distances between the Sun and Moon and other necessary data were computed from the topocentric coordinates of the Sun and of the Moon, calculated with the CERES software [*Chernetenko et al.*, 1992]. Differences in eclipse timing and occultation between the four locations along the line of sight were very small compared with instrument time resolution and other measurement uncertainties. Therefore eclipse circumstances calculated for the air mass directly above the PEARL-GBS are used in this work.

2.2. Retrieval of SCDs and VCDs Under a Changing Solar Spectrum

[9] PEARL-GBS data were analyzed using the differential optical absorption spectroscopy (DOAS) technique [e.g., *Noxon*, 1975; *Solomon et al.*, 1987] with the WinDOAS software [*Fayt and Roozendael*, 2001]. The eclipse caused the solar spectrum to change, complicating retrievals. Figure 2 shows the differential optical depth (DOD) before the eclipse (black) and at 96% occultation (gray). DOD is defined as

$$\mathrm{DOD}(\lambda) = \ln[I(\lambda)/I_o(\lambda)] - 3\mathrm{rd\ \ order\ \ polynomial}, \quad (1)$$

where λ is the wavelength, $I(\lambda)$ is the intensity at twilight, and $I_o(\lambda)$ is the intensity at noon. The polynomial is fit to the log ratio to remove low-frequency structure. The structure of the DOD before the eclipse is small and can be attributed to absorption of trace gases including ozone, NO_2, H_2O, and O_4, while the structure of the DOD at 96% totality has strong H, Fe, Mg, and Ca lines corresponding to the spectrum of the solar corona, as the central part of the solar disk is extinguished [*Pierce*, 1968]. The H_β line in this structure has approximately twice the DOD shown in the residuals in Figure 4 of *Gil et al.* [2000] for 95% occultation, which makes these retrievals more challenging. The effective temperature of the visible part of the solar disk also changes as the Moon covers the Sun, but the resulting change in the blackbody radiation curve [e.g., *Kazadzis et al.*, 2007] is removed with the polynomial in the DOAS technique.

[10] Ozone and NO_2 DSCDs were retrieved in WinDOAS [*Fayt and Roozendael*, 2001] with ozone [*Burrows et al.*, 1999], O_4 [*Greenblatt et al.*, 1990], NO_2 [*Vandaele et al.*, 1998], H_2O (converted from line parameters given in the work of *Rothman et al.* [2003]), and Ring pseudoabsorber [*Chance and Spurr*, 1997] cross sections. A reference spectrum from 17 July 2008 with a solar zenith angle (SZA) of 59° under cloudy skies was used, because it yielded the best DOAS fits over the course of the measurement period.

[11] In order to quantify the depths of the coronal features over the course of the solar eclipse, H_β (486.1 nm) and $H\gamma$ (434.0 nm) Balmer hydrogen line cross sections were constructed from the eclipse DOD in Figure 2 and added to the WinDOAS analyses for ozone and NO_2 in the usual fitting ranges of 450–545 and 425–450 nm, respectively. Figure 3 shows the DSCDs of the Balmer lines in arbitrary units. On

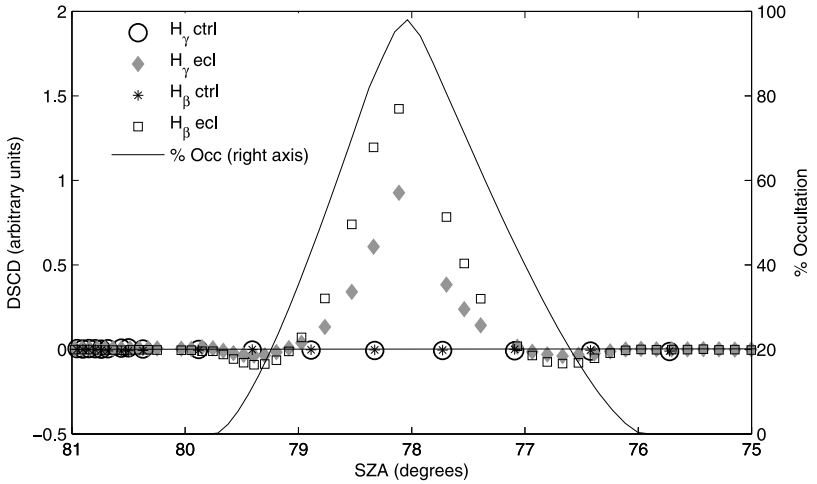

Figure 3. On the left axis, DSCDs in arbitrary units for $H\gamma$ on the morning before the eclipse (open circles) and the morning of the eclipse (gray diamonds) and H_β on the morning before the eclipse (black stars) and the morning of the eclipse (open squares). On the right axis, eclipse percentage occultation (black line).

the day before the eclipse, both the $H\gamma$ line DSCDs (open circles) and H_β line DSCDs (black stars) are negligible, which demonstrates that the Balmer line cross sections do not interfere with the regular DOAS fits. On the morning of the eclipse, the $H\gamma$ line DSCDs (gray diamonds) and H_β line DSCDs (open squares) follow the similar shapes. When the outer region of the solar disk is covered by the Moon (occultation less than 20%–30%), Balmer line DSCDs become negative. As more of the inner region of the solar disk is covered and the contribution from the chromosphere increases (occultation greater than 20%–30%), the Balmer line DSCDs become strongly positive. This agrees with *Gil et al.* [2000], who found that the transition between positive and negative Balmer line DSCDs occurred at ~20% occultation.

[12] In order to avoid the coronal lines, a number of DOAS fitting regions were tested. Ozone DSCDs were retrieved in a variety of fitting windows, including 450–545 nm (traditional fit window for the PEARL-GBS), 445–480 nm, 445–515 nm, and 445–550 nm with gaps from 480 to 490 nm and from 515 to 520 nm. Only DSCDs retrieved in the traditional ozone fitting region were stable on the day before the eclipse, likely because the DOD of ozone at the SZA of the eclipse (75°–80°) is small and affected by water absorption due to cloudy weather. Both H_β and Mg-Fe correction cross sections were tested on the data set. However, the broad structure of the Fe and Mg lines interfered with the DOAS retrievals on the noneclipse days. Therefore, only the H_β correction cross section was used. The resulting DOAS cross-section fits for ozone at SZA = 78°–79° are shown in Figure 4, with the DOAS fit in black and the data in gray. Ozone fits on the morning before the eclipse (Figure 4a) have random residuals. At 52% totality, the ozone fits (Figure 4b) still have fairly random residuals, showing only a small impact of the changed coronal spectrum. At 82% totality, the ozone fits (Figure 4c) show some systematic residuals around the wings of the H_β line and around the 517 nm Fe and Mg lines. When Balmer line cross sections are not fit in the ozone retrieval at 82% totality (Figure 4d), large systematic residuals dominate. Ozone DSCDs could not be retrieved for 96% totality because the coronal structure overwhelmed the residuals for this spectrum.

[13] NO_2 was also retrieved in a variety of fitting windows. The best root mean square residual before and during the eclipse was obtained for the 438–467 nm window, where there is less coronal structure, as is evident in Figure 2. Note that in the 438–467 nm window, no correction cross sections were necessary. The resulting fits for the traditional 425–450 nm range with $H\gamma$ correction cross section and this new fitting window are also shown in Figure 4. NO_2 DSCD fits are good on the day before the eclipse for both windows (Figure 4e and 4i). At 52% occultation, the advantages of the 438–467 nm window (Figure 4j) over the traditional window (Figure 4f) are apparent. At 82% occultation, the 438–467 nm window (Figure 4k) has some systematic errors but is much better than the traditional window (Figure 4g). The 425–450 nm fit is overwhelmed by the $H\gamma$ line when an $H\gamma$ correction cross section is not included (Figure 4h). Due to the reduced coronal interference in the 438–467 nm range, NO_2 could be retrieved for 96% occultation (Figure 4l).

[14] Ozone and NO_2 reference column densities (RCDs) were obtained using a Langley analysis [e.g., *Fraser et al.*, 2009] for the four twilights of 30 and 31 July 2008 in the 76°–81° SZA range, which was the lowest available SZA range for this time of year at Eureka. Eclipse day DSCDs were not included in the calculation of the RCD. Air mass factors (AMFs) were obtained from a one-dimensional radiative transfer model described in section 3.2. NO_2 AMFs were not chemically modified [e.g., *Roscoe et al.*, 2001]. However, this is expected to have a small impact on results as the modeled diurnal variation of NO_2 VCDs in the 76°–81° SZA range is less than 5%. To interpret the PEARL-GBS measurements, the SCDs (DSCD + RCD) from the morning before the eclipse were interpolated in

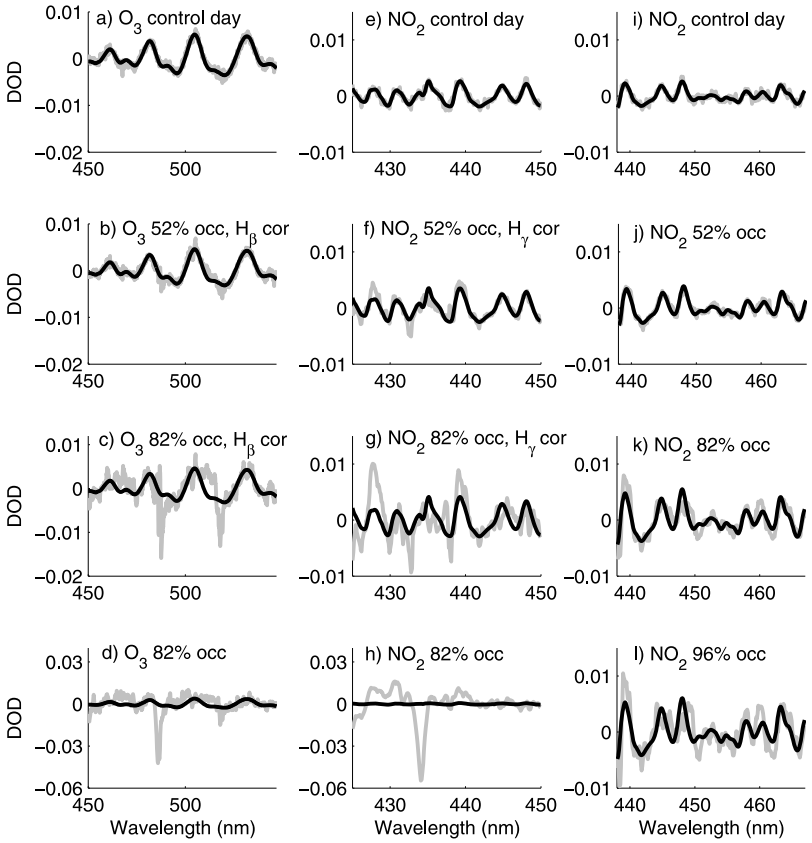

Figure 4. DOAS fits (black) and data (gray). For ozone in the 450–545 nm window (a) on the afternoon before the eclipse, (b) at 52% occultation, (c) at 82% occultation, and (d) at 82% occultation with no correction for H_β. For NO_2 in the 425–450 nm window (e) on the afternoon before the eclipse, (f) at 52% occultation, (g) at 82% occultation, and (h) at 82% occultation with no correction for $H\gamma$. For NO_2 in the 438–467 nm window (i) on the afternoon before the eclipse, (j) at 52% occultation, (k) at 82% occultation, and (l) at 96% occultation.

SZA to the eclipse day measurement grid and SCD ratios were taken. For ozone, VCDs throughout the twilight were also calculated with the formula,

$$\mathrm{VCD}(\theta_0) = (\mathrm{DSCD}(\theta_0) + \mathrm{RCD})/\mathrm{AMF}(\theta_0), \qquad (2)$$

where θ_0 is the SZA.

2.3. Estimates of Eclipse Systematic Errors in Ozone and NO_2 VCDs and DSCDs

[15] Previous DOAS studies during eclipses have not quantified the systematic changes in the fit residuals over the course of an eclipse. The error estimates used in this study are summarized in Table 1 for the measurements at 82% totality and on the previous morning, both at 78° SZA.

[16] Random, noneclipse systematic, and eclipse systematic errors all affect the DSCDs. Random fitting errors were calculated for each DSCD in WinDOAS and vary over the twilight. Systematic instrument, pseudorandom, absolute cross section, temperature dependence of cross section, and Raman scattering were estimated by *Fraser et al.* [2009] at 3.3% for ozone and 11.8% for NO_2 and are assumed to be consistent for all DSCDs.

[17] In order to estimate DSCD eclipse systematic errors, two tests were performed on the 82% occultation spectrum. In the first test, the residuals for the DOAS analysis of the 82% occultation spectrum were added to a spectrum from the previous day, which was then reanalyzed for ozone and NO_2. Ozone and NO_2 DSCDs changed by −6.4% and −3.7%, respectively, with the added residual. In the second test, the DSCDs of ozone and NO_2 at 82% occultation were retrieved for a variety of DOAS fit parameters, including modified Balmer line cross sections, wavelength calibration parameters, and offset corrections. Analyses in which these parameters significantly changed the DSCDs on the day before the eclipse or increased the DOAS root mean square residual values were omitted. For ozone, the largest variation was a 16% decrease in ozone DSCD, when a quadratic offset correction was added to the analysis. This was added in quadrature with the change observed in the first test. For NO_2, the 82% totality DSCD decreased by 31.4% and increased by 2.8%, when the fitting window was changed to 440–466 nm and 438–471 nm, respectively. These two values were each added in quadrature with 3.7% from the first test and taken as upper and lower NO_2 eclipse systematic DSCD errors. The eclipse systematic errors calculated for the 82% totality spectrum were scaled to the other measurements by the Balmer line DSCD strengths shown in Figure 3.

Table 1. Error Estimates for Ozone and NO_2 DSCDs, RCDs, and AMFs at 82% Occultation[a]

	O_3 Percentage Error at 82% Occultation [Same SZA on Noneclipse Morning]	NO_2 Percentage Error at 82% Occultation [Same SZA on Noneclipse Morning]
Random fitting error on DSCD: calculated in WinDOAS for each DSCD.	4.6 [1.2][b]	4.9 [3.2][b]
Non-eclipse systematic: same for all DSCDs, estimated by *Fraser et al.* [2009].	3.3 [3.3]	11.8 [11.8]
Eclipse DSCD systematic: calculated for 82% occultation by adding the following two tests in quadrature and scaled to other DSCDs by strength of Balmer lines	17.9 [0][b]	$^{+4.64}_{-31.6}$ [0][b]
1. Residual addition test	6.4 [0][b]	3.7 [0][b]
2. Analysis variation test	16.7 [0][b]	$^{+2.8}_{-31.4}$ [0][b]
RCD systematic error 1: due to noneclipse systematic error on DSCD.	3.3 [3.3]	11.8 [11.8]
RCD systematic error 2: from uncertainties in Langley plot; this is independent of other DSCD systematic errors	10.6 [10.6]	8.2 [8.2]
RCD systematic error 3: due to chemical changes in VCD over Langley plot SZA range	N/A	2.5 [2.5]
AMF random error: same for all spectra, estimated by *Bassford et al.* [2005]	2 [2]	5 [5]

[a]Square brackets indicate error estimate on morning before eclipse at same SZA as the eclipse.
[b]Error estimate calculated separately for each measurement.

[18] There are three RCD errors, all of which have a systematic effect on the data. The first RCD error is caused by the noneclipse systematic DSCD errors, which alter the slope of the Langley plot and thus the RCD by the same percentage. The second RCD error is from uncertainty in Langley plots and was taken as the standard deviation of the RCD values calculated from the four twilights. The third RCD error quantifies the effect of using AMFs that were not chemically modified for NO_2. This error was estimated at 2.5%, or half of the modeled NO_2 VCD variation in the SZA 76°–81° range. The second and third RCD errors are independent of DSCD systematic errors.

[19] The errors in DSCD, RCD, and AMF were propagated through the SCD ratio calculation and the VCD calculation in equation (2). The random errors were propagated using random error analysis formulae, with an AMF random error for ozone VCD calculations estimated at 2% by *Bassford et al.* [2005]. The systematic errors were each applied as upper and lower limits to the RCDs and DSCDs, and the resulting percentage changes in SCD ratio and VCD were calculated. For the SCD ratio, the 3.3% and 11.8% systematic errors apply equally to all DSCDs and RCDs and therefore cancel. The total errors for each measurement were calculated by adding all random and systematic errors in quadrature.

3. Modeling Ozone and NO_2 SCDs During an Eclipse

3.1. Ozone and NO_2 Ozone Profiles During an Eclipse

[20] Since ozone displays no diurnal variation below the uppermost stratosphere, a single ozone profile was used for all modeling studies. It was derived from an ozonesonde launched on the day of the eclipse and supplemented with an ozone climatology above 35 km [*McPeters et al.*, 2007]. This profile was held constant throughout the eclipse in the photochemical box model calculations.

[21] A photochemical box model [*McLinden et al.*, 2000; *Brohede et al.*, 2008] was used to simulate the evolution of NO_2 during the day of 1 August 2008 at Eureka (80°N). The model was constrained with measured ozone and temperature profiles from the ozonesonde described above, and NO_y from a climatology [*Brohede et al.*, 2008]. Profiles of NO and NO_2 were obtained from the model simulation between 10 and 52 km. Mixing ratios of NO and NO_2 below 10 km were set to the 10 km value at each time step. In this work, modeling of the NO_2 profile through an eclipse is based on the variation in the photolysis rate of NO_2 with the fraction of eclipse totality. This is outlined below.

[22] To a good approximation throughout most of the stratosphere, the ratio of NO_2 to NO_x (NO_x = NO + NO_2) can be obtained by considering the reactions,

$$NO_2 + h\nu \xrightarrow{J} NO + O, \tag{3}$$

$$NO + O_3 \xrightarrow{k} NO_2 + O_2. \tag{4}$$

Assuming a near steady state,

$$\frac{[NO_2]}{[NO_x]} = \frac{1}{1 + J/(k[O_3])} = \frac{1}{1 + r}, \tag{5}$$

where J is the NO_2 photodissociation rate constant, a function of available sunlight in the NO_2 photolysis region (~340–420 nm), and k is the NO + O_3 rate constant, where $[NO_2]$ and $[NO_x]$ are the number densities of NO_2 and NO_x, respectively. The quantity $r = J/(k[O_3])$ is the ratio of the first-order rate constants assuming ozone remains constant. The desired quantity r can be calculated from model calculations of NO_2 and NO_x,

$$r = \frac{1}{[NO_2]/[NO_x]} - 1. \tag{6}$$

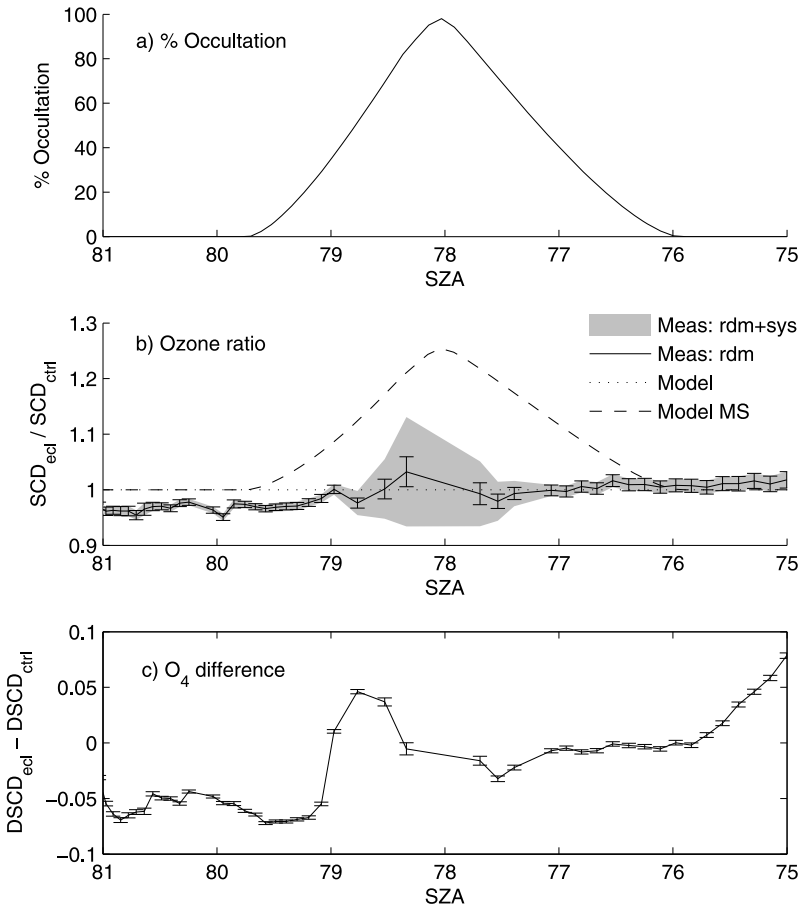

Figure 5. (a) Eclipse percentage occultation versus SZA. (b) Ozone eclipse SCD divided by control SCD with DOAS random fitting error (black with error bars) and combined fitting and eclipse systematic errors (gray shading), and modeled SCD difference for the standard atmosphere (dotted zero-line) and enhanced multiple scattering (black dashed line). (c) O_4 eclipse DSCD minus control DSCD, with random fitting error.

Note that by calculating r using full chemistry instead of simply using the model-calculated $J/(k[O_3])$ directly, other reactions that impact the NO_x partitioning, in particular $NO_2 + O(^3P)$, are accounted for.

[23] In this work r is a measure of the NO_x partitioning in the absence of an eclipse. The impact of the eclipse on photochemistry can be taken into account by adjusting the rate of NO_2 photolysis in a manner consistent with the varying sunlight. This is done by scaling r by the fraction of the solar disk that remains unocculted and is justified as the rates of both $NO_2 + h\nu$ (equation (3)) and $NO_2 + O(^3P)$ scale with the amount of available sunlight, the latter as the supply of $O(^3P)$ is largely controlled by the photolysis of O_3. In this case, NO_2 through an eclipse can be expressed as

$$[NO_2] = \frac{[NO_x]}{1 + r(1-\gamma)}, \tag{7}$$

where γ represents the eclipse fraction, as shown in Figures 5, 6, and 7, and r was calculated using equation (6). Equation (7) is simply equation (5) with a scaling applied to the rate of NO_2 destruction. When $\gamma = 0$ or no eclipse, NO_2 is at its normal level, but for a total eclipse, $\gamma = 1$, then $[NO_2] = [NO_x]$.

[24] The brightness of the Sun, and thus the available sunlight for photolysis, varies across the solar disk. Therefore, an additional limb darkening correction is applied to γ, based on the calculations of *Koepke et al.* [2001], using their values at 390 nm to represent the NO_2 photolysis region.

3.2. Modeling of Slant Column Densities

[25] Slant column densities of ozone and NO_2 are modeled using the general expression,

$$\mathrm{SCD}(\theta_0) = \Sigma \mathrm{AMF}(z, \theta_0)[X](z, \theta_0)\Delta z, \tag{8}$$

where z is altitude, θ_0 is SZA, $[X]$ is the number density of ozone $[O_3]$ or NO_2 $[NO_2]$, Δz is layer thickness, and the summation is over altitude layers. The AMF describes the enhancement in absorption due to light traversing a slant path through a layer and is calculated using the multiple-scattering radiative transfer model of *McLinden et al.* [2002, 2006]. Calculations are performed using a surface albedo of

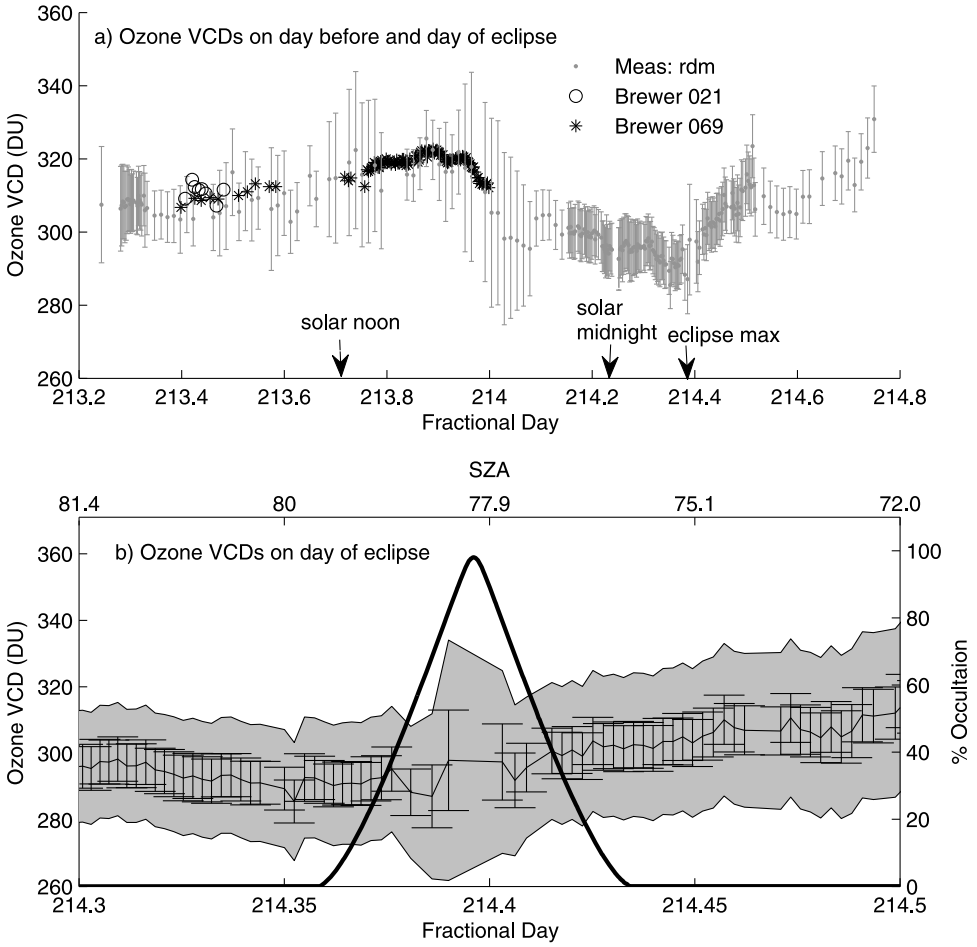

Figure 6. (a) Ozone VCDs for the day preceding the eclipse and the eclipse morning versus fractional day measured by the PEARL-GBS with random error (gray with error bars), Brewer 021 (black open circles), and Brewer 069 (black stars). (b) PEARL-GBS ozone VCDs during eclipse versus fractional day (bottom axis) and SZA (top axis) during eclipse with random error (black with error bars) and combined eclipse systematic and random errors (gray shading) plotted with the eclipse percentage occultation on the right axis (black line).

0.1 and a wavelength of 500 nm for ozone and 452 nm for NO_2 to correspond with the wavelengths regions in which ozone and NO_2 were retrieved. Using these AMFs, ozone SCDs were calculated using the sonde-measured ozone profile and NO_2 SCDs from the model-calculated profile described above.

[26] During an eclipse, the fraction of multiple-scattered light should increase [*Shaw*, 1978; *Emde and Mayer*, 2007]. This is due to a larger relative contribution of diffuse light from neighboring air masses that are experiencing a smaller (or zero) eclipse fraction. To assess how this might impact the overall AMF, a total eclipse AMF is defined that is calculated considering only multiple-scattered light. An eclipse AMF can then be defined as,

$$\mathrm{AMF_e} = (1-\gamma)\mathrm{AMF_{std}} + \gamma\mathrm{AMF_{ms}}, \quad (9)$$

where $\mathrm{AMF_{std}}$ is the standard AMF and $\mathrm{AMF_{ms}}$ is the AMF calculated considering only multiple-scattered light. The assumed linear combination implies that during a total eclipse, only multiple-scattered light is measured.

4. Results and Discussion

4.1. Radiative Transfer During the Eclipse

[27] To aid in the interpretation of the PEARL-GBS measurements during the eclipse, the SCDs from the previous morning were interpolated in SZA to the eclipse day measurement grid; these measurements will be called the control data. Ozone SCD measurements derived from the 450–545 nm region are shown in Figure 5. Figure 5a shows the eclipse percentage occultation versus SZA, calculated using the method described in section 2.1. In Figure 5b, the ratio between the eclipse and control ozone SCDs are plotted with the random fitting error only (black with error bars) and for combined fitting and eclipse systematic errors caused by the changing solar spectrum (gray shading) and show no significant changes in ozone caused by the eclipse.

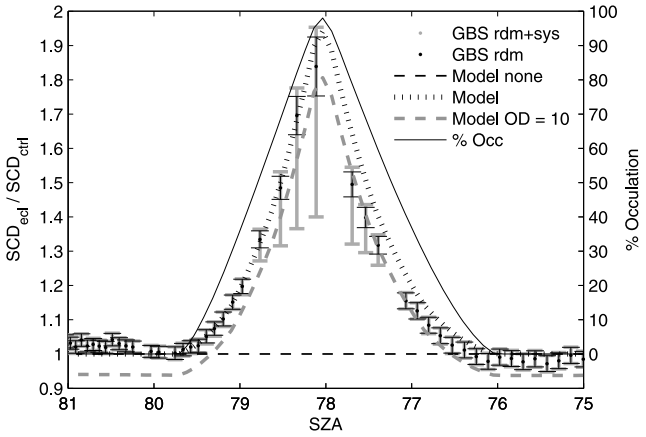

Figure 7. On the left *y* axis, ratio of eclipse NO_2 SCD to control SCD measured with the PEARL-GBS with systematic and random errors (gray with error bars) and random errors only (black with error bars), and the modeled SCD ratio for no eclipse (black dashed zero line), eclipse with no clouds (black dotted line), and eclipse with optical depth 10 (gray dashed line). On the right axis, the eclipse percentage occultation is shown (thick black line).

[28] Theoretically, toward an eclipse maximum, contributions from multiple-scattered light dominate in the zenith-viewing direction [*Shaw*, 1978; *Emde and Mayer*, 2007]. Therefore the AMFs were derived for both the standard atmosphere and for increased multiple scattering toward eclipse maximum, as discussed in section 3.2, then applied to modeled ozone profiles to calculate SCDs, and are shown in Figure 5b. The modeled difference in ozone SCDs calculated with the standard AMFs (dotted line) is a constant value of one as there are no photochemical changes in ozone over the short time period of the eclipse. The SCD ratio for the multiple-scattering AMFs (dashed line) is positive as the multiple-scattering AMFs tend to be about 20% larger than the standard AMFs at eclipse maximum. The multiple-scattering AMFs are outside the uncertainty range of the SCD difference, suggesting that this has a small effect up to 82% occultation.

[29] O_4 SCDs can also be used as a proxy for changing radiative transfer [e.g., *Wagner et al.*, 2002]. In Figure 5c, the difference between eclipse and control O_4 DSCDs measured in the 450–545 nm range are shown in black with fitting error. The DSCD ratio was not plotted due to near-zero O_4 DSCDs in the denominator. O_4 increases over the morning of the eclipse, likely due to the incoming rain clouds, but does not appear to be correlated with the eclipse occultation, suggesting that the eclipse is not significantly affecting the path of light to the instrument.

[30] There is no evidence of enhanced multiple-scattering in the O_4 or ozone measurements. This is likely because ozone measurements were all taken more than ten minutes away from the eclipse maximum. In a modeling study, *Emde and Mayer* [2007] found that diffuse radiation does not contribute significantly to zenith-scattered light outside ±10 min of a total eclipse at SZA 35°. Their study was performed for much higher Sun and therefore is not directly applicable to this work but demonstrates that away from eclipse maximum, the impact of diffuse radiation can drop off quickly. Because there was no evidence of enhanced multiple scattering in this study, standard AMFs were therefore used.

4.2. Variability of Ozone VCDs During the Eclipse

[31] In Figure 6a, PEARL-GBS ozone VCDs are plotted against the fractional day (gray with error bars) for the day before and the morning of the eclipse. Two Brewer spectrometers are located at Eureka, Brewer 021 (a MKIII double-Brewer) and 069 (a MKII single-Brewer) [e.g., *Savastiouk and McElroy*, 2005] and their direct Sun VCDs are shown in black open circles and black stars, respectively. Good agreement is evident. In Figure 6b, the VCDs during the eclipse measured by the PEARL-GBS are shown in more detail with random error (black with error bars) and combined eclipse systematic and random errors (gray shading) and are plotted against fractional day (bottom *x* axis) and SZA (top *x* axis). On the right *y* axis, the percentage occultation of the eclipse is plotted (thick black line). Ozone VCDs from the Brewer spectrometers during the eclipse are not shown as they have not been corrected for the change in the solar spectrum and hence are unreliable.

[32] Over the 2 h of the eclipse, ozone VCDs measured with the PEARL-GBS rose at a rate of 7.0 ± 0.5 DU/h. The gradual increase in ozone over the course of the eclipse could be due to natural variability, as a 10.3 ± 1.2 DU/h drop in ozone was measured over a two-hour period on the previous afternoon. Two possible ozone oscillations occur between approximately 30%–80% occultation on either side of eclipse totality, with ~2%–3% amplitudes and ~20 min periods. These are consistent with ozone oscillations measured by *Zerefos et al.* [2007], who found 2.5%–3% amplitude oscillations with periods of 30–40 min and *Chakrabarty et al.* [1997], who found ~5% amplitude oscillations with periods of ~15 min. However, the oscillations are not significant above the combined random and systematic errors, which run from 3.3% to 6.8% over the eclipse. Also, only four measurements make up each oscillation and the 19 min time period around maximum eclipse occultation was not sampled. Therefore, this study is inconclusive regarding ozone oscillations.

4.3. NO_2 During the Eclipse: Measurements and Models

[33] NO_2 shows a much stronger variability during the eclipse. The measured ratios between eclipse and control NO_2 SCDs were calculated and multiplied by 1.07 to account for day-to-day variability in NO_2. These are shown on the left *y* axis of Figure 7, with fitting error (black with error bars) and combined fitting error and eclipse systematic error (gray with error bars) indicated. The measurements increase and decrease with eclipse occultation (thick black line on right *y* axis). The ratio of the maximum measured SCD, at 96% occultation, to the SCD measured at the same SZA on the previous morning was $1.84^{+0.12}_{-0.43}$.

[34] NO_2 profiles were modeled for 09:30 UT (04:30 LT), the time of the eclipse maximum, for normal levels of sunlight and for reduced sunlight during the eclipse. For normal sunlight, the corresponding VCD was 4.75×10^{15} mol/cm^2, while at eclipse maximum, it was 9.18×10^{15} mol/cm^2. Modeled VCDs were converted to SCDs and a ratio of eclipse to noneclipse SCDs was taken. This ratio is shown in Figure 7

Table 2. Measurements NO_2 During Eclipses From Past Studies Compared With Calculations Using the Eclipse Photochemical Model From This Study

	Eclipse Date	Measured Quantity	Latitude	Occultation	SZA	Measurement	Model
This work	01 Aug 2008	Ratio of eclipse to noneclipse SCD	80°N	96%	78° am	$1.84^{+0.12}_{-0.43}$	1.91
Gil et al. [2000]	26 Feb 1998	Ratio of eclipse to noneclipse SCD	28°N	95%	92° pm	1.55 ± 0.09	1.47
Elansky and Elokhov [1993]	22 Jul 1990	Ratio of eclipse to noneclipse VCD	61°N	99.7%	87° am	1.55 ± 0.06	1.55
Elansky and Arabov [1983], *Elansky and Elokhov* [1993]	31 Jul 1981	Ratio of eclipse to noneclipse VCD	44°N	92.5%	82° am	1.6 ± 0.2	1.72

for the eclipse under cloud-free conditions (black dotted line). The modeled ratio agrees well with the data up until the eclipse maximum. For the second half of the eclipse, the measurements follow the same shape as the model, but are systematically lower than the model. This asymmetry may be introduced by multiple scattering in clouds [*Pfeilsticker et al.*, 1998] as cloudy conditions varied over the course of the eclipse. AMFs were also calculated for an optical depth of 10 and the resulting SCD ratio is shown in Figure 7 (gray dashed line). These cloudy-weather AMFs were found to change the modeled SCD ratio by 6%–7%, which could account for the discrepancies between the model and measurements. Furthermore, at Eureka, the tropospheric SCD is about 5% of the total SCD. Therefore, errors of 40% in the modeled tropospheric NO_2 density would impact the overall modeled SCD at the 2% level. The model suggests an SCD ratio of 1.91 at 96% occultation for cloud-free conditions.

[35] In an effort to compare these results to results from previous studies, which were measured for different times of year, eclipse totalities, locations, and SZAs, the eclipse model was applied to previous eclipse studies and the results are summarized in Table 2. These simulations were carried out in an identical manner to this study except that climatologies were used for the ozone [*McPeters et al.*, 2007] and temperature [*Nagatani and Rosenfield*, 1993] in the box model. In all cases, the modeled SCD and VCD ratios agree within uncertainty with the studies. This demonstrates a high level of consistency considering the range of latitudes and SZAs at which the eclipses occurred. It was found that aside from eclipse totality, the main factor affecting the ratio was the SZA. At large SZA, much of the NO_x is already in NO_2, so there is less NO_x available for conversion to NO_2. Therefore, due to the smaller SZA (higher-Sun) of 78°, this study measures a larger increase in NO_2 in than in past studies.

5. Conclusion and Summary of Results

[36] During the 98% totality 1 August 2008 solar eclipse, ozone and NO_2 were measured using the PEARL-GBS, a UV-visible ground-based spectrometer at Eureka, Canada. DSCD retrievals were complicated by the small SZA of the measurements (75°–80°) and the changing solar spectrum during the eclipse. The changes in the solar spectrum were explored and fitting parameters were optimized to reduce the impact of the coronal spectrum. Eclipse systematic errors were estimated to account for added structure in the DOAS fitting residuals. With improved DOAS analysis settings, ozone was retrieved up to 82% occultation and NO_2 was retrieved up to 96% occultation.

[37] Radiative transfer up to 82% occultation was studied with O_4 DSCDs and a radiative transfer model with enhanced multiple scattering. It was found that the eclipse had little impact on radiative transfer for zenith-scattered sunlight up to 82% totality.

[38] Ozone VCDs were retrieved and a gradual increase in ozone throughout the eclipse was found to be within the natural variability of ozone at Eureka. Due to measurement errors and the limited temporal resolution of the data, no conclusion could be drawn about ozone oscillations although there was some evidence of two oscillations with amplitude of 2%–3% and a 20 min period.

[39] Measured eclipse and control day NO_2 SCDs were found to have a peak ratio of $1.84^{+0.12}_{-0.43}$, which agrees with the modeled value of 1.91. The NO_2 eclipse model was applied to the eclipse totalities, locations, and SZA of the measurements of *Gil et al.* [2000], *Elansky and Elokhov* [1993], and *Elansky and Arabov* [1983] and was found to be in good agreement with these studies. Due the large eclipse occultation and the small SZA of this study, the NO_2 SCD ratio from this study was the largest of past measurements.

[40] **Acknowledgments.** The Polar Environment Atmospheric Research Laboratory (PEARL) is operated by the Canadian Network for the Detection of Atmospheric Change (CANDAC). CANDAC/PEARL funding partners are the Arctic Research Infrastructure Fund, Atlantic Innovation Fund/Nova Scotia Research Innovation Trust, Canadian Foundation for Climate and Atmospheric Science, Canadian Foundation for Innovation, Canadian Space Agency, Environment Canada, Government of Canada International Polar Year, Natural Sciences and Engineering Research Council, Ontario Innovation Trust, Ontario Research Fund, Indian and Northern Affairs Canada, and the Polar Continental Shelf Program. Thanks to CANDAC/PEARL Principal Investigator James R. Drummond, PEARL Operations Manager Pierre Fogal, and all of the CANDAC operators who have helped with GBS measurements at PEARL, particularly Oleg Mikhailov and Matthew Mahoney, who took measurements with the PEARL-GBS during the solar eclipse. Thanks also to Rebecca Batchelor for her invaluable help coordinating the eclipse measurements at Eureka. WinDOAS was kindly provided by Caroline Fayt and Michel Van Roozendael of the Belgian Institute for Space Aeronomy (IASB-BIRA). Thanks to the staff at the Eureka Weather station for their hospitality and ozonesonde launches. Weather, Brewer, and ozonesonde data were provided by Environment Canada. The eclipse map is courtesy of Fred Espenak and Jay Anderson, "Total Solar Eclipse of 2008 August 01" (NASA/TP-2007-214149).

References

Abalakin, V. K. (Ed.) (1981), *Astronomical Calendar - Constant Part*, Science Publishing House, Moscow.

Bassford, M. R., K. Strong, C. A. McLinden, and C. T. McElroy (2005), Ground-based measurements of ozone and NO_2 during MANTRA 1998 using a Zenith-sky spectrometer, *Atmos.-Ocean.*, *43*, 325–338.

Bojkov, R. D. (1968), Ozone variations during solar eclipse of 20 May 1966, *Tellus*, *20*, 417–421.

Brohede, S., C. A. McLinden, J. Urban, C. S. Haley, A. I. Jonsson, and D. Murtagh (2008), Odin stratospheric proxy NO_y measurements and climatology, *Atmos. Chem. Phys.*, *8*, 5731–5754.

Burrows, J. P., A. Richter, A. Dehn, B. Deters, S. Himmelmann, and J. Orphal (1999), Atmospheric remote-sensing reference data from GOME:

2. Temperature-dependent absorption cross sections of O-3 in the 231-794 nm range, *J. Quant. Spectrosc. Radiat. Transfer*, *61*, 509–517.
Chakrabarty, D. K., S. K. Peshin, S. K. Srivastav, N. C. Shah, and K. V. Pandya (2001), Further evidence of total ozone variation during the solar eclipse of 1995, *J. Geophys. Res.*, *106*, 3213–3218, doi:10.1029/2000JD900522.
Chakrabarty, D. K., N. C. Shah, and K. V. Pandya (1997), Fluctuation in ozone column over Ahmedabad during the solar eclipse of 24 October 1995, *Geophys. Res. Lett.*, *24*(23), 3001–3003, doi:10.1029/97GL03016.
Chance, K. V., and R. J. D. Spurr (1997), Ring effect studies: Rayleigh scattering, including molecular parameters for rotational Raman scattering, and the Fraunhofer spectrum, *Appl. Opt.*, *36*, 5224–5230.
Chernetenko, Y. A., V. N. L'vov, V. A. Shor, R. I. Smekhacheva, and S. D. Zeckmeister (1992), CERES: The integrated software package for minor planets research, paper presented at Second International Workshop on Positional Astronomy and Celestial Mechanics, Spain.
Chimonas, G., and C. O. Hines (1971), Atmospheric gravity waves induced by a solar eclipse, 2, *J. Geophys. Res.*, *76*(28), 7003–7005, doi:10.1029/JA076i028p07003.
Dani, K. K., and P. C. S. Devara (2002), Aerosol optical depth and ozone variations during the total solar eclipse of 24 October 1995, *Atmos. Res.*, *65*(1–2), 1–15.
Eckermann, S. D., D. Broutman, M. T. Stollberg, J. Ma, J. P. McCormack, and T. F. Hogan (2007), Atmospheric effects of the total solar eclipse of 4 December 2002 simulated with a high-altitude global model, *J. Geophys. Res.*, *112*, D14105, doi:10.1029/2006JD007880.
Elansky, N. F., and A. Y. Arabov (1983), Measurements of nitrogen dioxide content in the atmosphere during the solar eclipse of July 31, 1981, *Izv. Acad. Sci. USSR Atmos. Oceanic Phys. Eng. Trans.*, *18*, 511–513.
Elansky, N. F., and A. S. Elokhov (1993), Variation of stratospheric NO_2 during the solar eclipse, in *Ozone in the Troposphere and the Stratosphere, Part 2*, *NASA Conf. Publ. 326*, *Proc. of 1992*, *Quadrenn. Ozone Symp.*, 3266, 699–702.
Emde, C., and B. Mayer (2007), Simulation of solar radiation during a total eclipse: A challenge for radiative transfer, *Atmos. Chem. Phys.*, *7*, 2259–2270.
Espenak, F., and J. Anderson (2007), Total solar eclipse of 2008 August 01, *NASA Technical Publication*, *214149*.
Fayt, C., and M. V. Roozendael (2001), *WinDOAS 2.1—Software User Manual*, Uccle, Belgium.
Fraser, A., C. Adams, J. R. Drummond, F. Goutail, G. Manney, and K. Strong (2009), The Polar Environment Atmospheric Research Laboratory UV-visible ground-based spectrometer: First measurements of O_3, NO_2, BrO, and OClO columns, *J. Quant. Spectrosc. Radiat. Transfer*, *110*, 986–1004, doi:10.1016/j.jqsrt.2009.02.034.
Fraser, A., et al. (2008), Intercomparison of UV-visible measurements of ozone and NO_2 during the Canadian Arctic ACE validation campaigns: 2004–2006, *Atmos. Chem. Phys.*, *8*, 1763–1788.
Fritts, D. C., and Z. G. Luo (1993), Gravity-wave forcing in the middle atmosphere due to reduced ozone heating during a solar eclipse, *J. Geophys. Res.*, *98*(D2), 3011–3021, doi:10.1029/92JD02391.
Gil, M., O. Puentedura, M. Yela, and E. Cuevas (2000), Behavior of NO_2 and O_3 columns during the eclipse of February 26, 1998, as measured by visible spectroscopy, *J. Geophys. Res.*, *105*(D3), 3583–3593, doi:10.1029/1999JD900973.
Greenblatt, G. D., J. J. Orlando, J. B. Burkholder, and A. R. Ravishankara (1990), Absorption-measurements of oxygen between 330nm and 1140nm, *J. Geophys. Res.*, *95*(D11), 18,577–18,582, doi:10.1029/JD095iD11p18577.
Herman, J. R. (1979), Response of stratospheric constituents to a solar eclipse, sunrise, and sunset, *J. Geophys. Res.*, *84*(C7), 3701–3710, doi:10.1029/JC084iC07p03701.
Kazadzis, S., A. Bais, M. Blumthaler, A. Webb, N. Kouremeti, R. Kift, B. Schallhart, and A. Kazantzidis (2007), Effects of total solar eclipse of 29 March 2006 on surface radiation, *Atmos. Chem. Phys.*, *7*, 5775–5783.
Koepke, P., J. Reuder, and J. Schween (2001), Spectral variation of the solar radiation during an eclipse, *Meteorol. Z.*, *10*, 179–186.
McLinden, C. A., C. S. Haley, and C. E. Sioris (2006), Diurnal effects in limb scatter observations, *J. Geophys. Res.*, *111*, D14302, doi:10.1029/2005JD006628.
McLinden, C. A., J. C. McConnel, E. Griffioen, and C. T. McElroy (2002), A vector radiative-transfer model for the Odin/OSIRIS project, *Can. J. Phys.*, *80*(4), 375–393, doi:10.1139/P01-156.
McLinden, C. A., S. C. Olsen, B. Hannegan, O. Wild, M. J. Prather, and J. Sundet (2000), Stratospheric ozone in 3-D models: A simple chemistry and the cross-tropopause flux, *J. Geophys. Res.*, *105*(D11), 14,653–14,665, doi:10.1029/2000JD900124.
McPeters, R. D., G. J. Labow, and J. A. Logan (2007), Ozone climatological profiles for satellite retrieval algorithms, *J. Geophys. Res.*, *112*, D05308, doi:10.1029/2005JD006823.
Mims, F. M., and E. R. Mims (1993), Fluctuations in column ozone during the total solar eclipse of July 11, 1991, *Geophys. Res. Lett.*, *20*(5), 367–370, doi:10.1029/93GL00493.
Nagatani, R. M., and J. E. Rosenfield (1993), Temperature, net heating and circulation, in *The Atmospheric Effects of Stratospheric Aircraft: Report of the 1992 Models and Measurements Workshop*, *NASA Ref. Publ. 1292*, edited by M. J. Prather and E. E. Remsberg, pp. A1–A47.
Noxon, J. F. (1975), Nitrogen-dioxide in stratosphere and troposphere measured by ground-based absorption spectroscopy, *Science*, *189*, 547–549.
Pfeilsticker, K., F. Erle, O. Funk, L. Marquard, T. Wagner, and U. Platt (1998), Optical path modifications due to tropospheric clouds: Implications for zenith sky measurements of stratospheric gases, *J. Geophys. Res.*, *103*(D19), 25,323–25,335, doi:10.1029/98JD01803.
Pierce, A. K. (1968), Chromospheric spectrum outside of eclipse $\lambda\lambda$ 3040 to 9266 A°, *Astrophys. J. Suppl. Ser.*, *17*, 1–370.
Pommereau, J. P., A. Hauchecorne, and G. Souchon (1976), Variation of atmospheric NO_2 total content observed during a solar eclipse – diurnal-variation in tropics, *C. R. Seances Acad. Sci., Ser. B*, *283*, 163–165.
Roscoe, H. K., A. J. Charlton, D. J. Fish, and J. G. T. Hill (2001), Improvements to the accuracy of measurements of NO_2 by zenith-sky visible spectrometers: II. Errors in zero using a more complete chemical model, *J. Quant. Spectrosc. Radiat. Transfer*, *68*, 337–349.
Rothman, L. S., et al. (2003), The HITRAN molecular spectroscopic database: Edition of 2000 including updates through 2001, *J. Quant. Spectrosc. Radiat. Transfer*, *82*(1–4), 5–44, doi:10.1016/S0022-4073(03)00146-8.
Savastiouk, V., and C. T. McElroy (2005), Brewer spectrophotometer total ozone measurements made during the 1998 Middle Atmosphere Nitrogen Trend Assessment (MANTRA) campaign, *Atmos.-Ocean*, *43*, 315–324.
Shaw, G. E. (1978), Sky radiance during a total solar eclipse – theoretical model, *Appl. Opt.*, *17*, 272–276.
Solomon, S., A. L. Schmeltekopf, and R. W. Sanders (1987), On the interpretation of zenith sky absorption-measurements, *J. Geophys. Res.*, *92*(D7), 8311–8319, doi:10.1029/JD092iD07p08311.
Starr, W. L., R. A. Craig, M. Loewenstein, and M. E. McGhan (1980), Measurements of NO, O_3, and temperature at 19.8 km during the total solar elipse of 26 February 1979, *Geophys. Res. Lett.*, *7*(7), 553–555, doi:10.1029/GL007i007p00553.
Vandaele, A. C., C. Hermans, P. C. Simon, M. Carleer, R. Colin, S. Fally, M. F. Merienne, A. Jenouvrier, and B. Coquart (1998), Measurements of the NO_2 absorption cross-section from 42 000 cm^{-1} to 10 000 cm^{-1} (238-1000 nm) at 220 K and 294 K, *J. Quant. Spectrosc. Radiat. Transfer*, *59*, 171–184.
Wagner, T., C. von Friedeburg, M. Wenig, C. Otten, and U. Platt (2002), UV-visible observations of atmospheric O_4 absorptions using direct moonlight and zenith-scattered sunlight for clear-sky and cloudy sky conditions, *J. Geophys. Res.*, *107*(D20), 4424, doi:10.1029/2001JD001026.
Wuebbles, D., and J. S. Chang (1979), Theoretical-study of stratospheric trace species variations during a solar eclipse, *Geophys. Res. Lett.*, *6*(3), 179–182, doi:10.1029/GL006i003p00179.
Zerefos, C. S., et al. (2000), Changes in surface solar UV irradiances and total ozone during the solar eclipse of August 11, 1999, *J. Geophys. Res.*, *105*(D21), 26,463–26,473, doi:10.1029/2000JD900412.
Zerefos, C. S., et al. (2007), Evidence of gravity waves into the atmosphere during the March 2006 total solar eclipse, *Atmos. Chem. Phys.*, *7*, 4943–4951.

C. Adams and K. Strong, Department of Physics, University of Toronto, 60 St. George St., Toronto, ON, M5S 1A7, Canada. (cadams@physics.utoronto.ca)
C. A. McLinden, Environment Canada, Toronto, ON, M3H 5T4, Canada.
V. Umlenski, Bulgarian Academy of Sciences, Institute of Astronomy, 72 Tzarigradsko Shaussee Blvd., BG-1784 Sofia, Bulgaria.